Distinct HAND2/HAND2-AS1 Expression Levels Finetune Mesenchymal and Epithelial Cell Plasticity in Human Mesenchymal Stem Cells

Rachel Vazana-Netzarim , Yishay Elmalem , Shachar Sofer , Hod Bruck , Naama Danino , Udi Sarig *

Posted Date: 26 September 2023

doi: 10.20944/preprints202309.1783.v1

Keywords: human mesenchymal stem cells; mesenchymal to epithelial transition (MET); epithelial to mesenchymal transition (EMT); HAND2; HAND2-AS1; senescence; stem cell plasticity

Article

Distinct HAND2/HAND2-AS1 Expression Levels Finetune Mesenchymal and Epithelial Cell Plasticity in Human Mesenchymal Stem Cells

Racheli Vazana-Netzarim [1], Yishay Elmalem [2], Shachar Sofer [2], Hod Bruck [2], Naama Danino [1] and Udi Sarig [1,2,*]

The Dr. Miriam and Sheldon Adelson School of Medicine, Department of Morphological Sciences and Teratology, Ariel University.

Department of Chemical Engineering and Biotechnology, Faculty of Engineering, Ariel University.

* Correspondence: Corresponding Author: Dr. Udi Sarig, PhD, Head–The Laboratory for Advanced Tissue Technologies (LATi-Tech), Department of Morphological Sciences and Teratology, Dr. Miriam and Sheldon Adelson School of Medicine, Ariel University, Ariel, 4070000, Israel, Email: udis@ariel.ac.il

Abstract: We have previously developed several successful decellularization strategies yielding porcine cardiac extracellular matrices (pcECMs), which exhibit tissue-specific bioactivity and bioinductive capacity when cultured with various pluri- and multipotent stem cells. Here we studied the tissue-specific effects of the pcECM on seeded human mesenchymal stem cells (hMSCs) phenotype using reverse transcribed quantitative polymerase chain reaction (RT-qPCR) arrays for cardio-vascular related genes. We further corroborated interesting findings at the protein level (flow cytometry and immunological stains) as well as bioinformatically using several mRNA sequencing and protein databases of normal and pathologic adult tissue expression, as well as during human embryonic organogenesis. We discovered that upon seeding of human mesenchymal stem cells (hMSCs) on the pcECM they displayed partial MET toward endothelial phenotypes ($CD31^{+}$) and morphologies, which were preceded by an early spike (~day 3 onward after seeding) in HAND2 expression at both the mRNA and protein levels compared to plate controls. CRISPR-Cas9 knockout (KO) of HAND2 and its associated antisense long non-coding RNA (HAND2-AS1) regulatory region resulted in proliferation arrest, hypertrophy, and senescent-like morphology. Bioinformatic analyses revealed that HAND2 and HAND2-AS1 are highly correlated in expression, are expressed in many different tissue types albeit at distinct yet tightly regulated expression levels. Deviation (down or up regulation) from these basal tissue expression levels are associated with a long list of pathologies. We thus suggest that HAND2 expression levels may finetune cell plasticity possibly affecting senescence and mesenchymal-to-epithelial transition states, through yet unknown mechanisms. Targeting this pathway may represent a promising new therapeutic approach for a wide range of diseases, including cancer, degenerative disorders, and aging. Nevertheless, further investigations are required to better understand the molecular players involved, potential inducers and inhibitors of this pathway, and eventually potential therapeutic applications.

Keywords: human mesenchymal stem cells; mesenchymal to epithelial transition (MET); epithelial to mesenchymal transition (EMT); HAND2; HAND2-AS1; senescence; stem cell plasticity

1. Introduction

Two key processes guiding tissue and organ development both during embryogenesis and in various pathophysiological contexts are epithelial-to-mesenchymal transition (EMT) and its reverse mesenchymal-to-epithelial transition (MET)[1]. Epithelial cells form stationary barriers delineating tissues and organs[2], create lumen and tube morphologies (e.g., via 'hollowing' and 'cavitation'[3]), maintain basal–apical cell polarity by basement membrane (BM) anchoring, and ensure strict cell–cell contact through desmosomes, gap-, adherens-, and tight-junctions[4]. Mesenchymal cells, in contrast, are spindle shaped, reside within, and remodel the 3D fibrous extracellular matrix (ECM), and can travel long distances while invading tissues within the body[2,5]. The epithelial-to-mesenchymal spectrum is wide, and contains many intermediate phenotypes[6].

Cell state transitioning (both EMT and MET) is crucial for tissue and organ development and is vital for almost every step of embryogenesis, including extraembryonic trophectoderm specification, embryonic gastrulation, body-plan patterning and, ultimately, organogenesis (establishment and diversification of body organs)[5,7-9]. For example, neural crest cells (NCCs) delaminate via EMT from the neural plate border and migrate to distant embryonic destinations[7,10,11] including the pharyngeal arches[12], head and neck mesenchyme[11], second heart field[13], and adrenal gland medulla[14]. Upon reaching their destinations, NCCs undergo at least one more MET to assume parenchymal differentiated cell states and morphologies[9].

Moreover, EMT and MET are also of paramount importance for adult tissue homeostasis and regeneration[15], and are involved in numerous pathological conditions including cancer metastasis[16], fibrosis during aging[2], cellular senescence[17,18] and MET mediated escape from senescence[19]. In essence, most tissue formation and remodeling processes necessitate at least one EMT-MET cycle, making the study of these processes critical not only for developmental biology and tissue engineering purposes but also for better understanding of pathologies and possible therapy development.

Global, often antagonistic, cellular programs ensure the protection of epithelial-mesenchymal homeostasis—including specific splicing, miRNA regulatory networks and other epigenetic mechanisms, which are still not completely understood (particularly, for MET)[1,5]. Direct human organogenesis embryo models, however, are notoriously difficult to generate (also limited by the '14-day' ethical rule)[20], and EMT/MET regulatory network manipulation is, in many cases, lethal. Hence, current EMT/MET knowledge is mostly deduced from animal models (i.e., drosophila, chick, zebrafish, and murine)[9], and by employing human cancer cell spheroids and/or human primary and stem cell-derived models[21-23].

One possible downstream common mediator of MET may be heart and neural crest derivatives 2 (HAND2), a type B basic helix-loop-helix (bHLH) transcription factor (TF)[24], and its associated anti sense long non-coding RNA (lncRNA, HAND2-AS1). Embryonically, HAND2 induces type 1 (embryonic) MET patterning of NCCs to branching aortic vessels and of mesodermal second heart field (SHF) cells to the right ventricle (RV), parts of the atria, interventricular septum, and outflow tract[25-27]. HAND2 murine knockout (KO) is lethal at E9.5-10.5, yielding RV hypoplasia, single chambered hearts, and vascular malformations[25,28]. Molecularly, HAND2 is a crucial downstream regulator of the endocardial VEGF-Notch signaling pathway during cardiogenesis and coronary vasculogenesis[27]. HAND2 also instructs type 1 MET in anterior-posterior limb-bud digit patterning (initiating a SHH/FGF feedback loop)[29] and induces embryonic mesothelium progenitor formation delineating internal organs and contributing to organogenesis, tissue homeostasis and regeneration, through unclear signaling[30]. HAND2 was, thus, suggested as a "regulator of tissue morphogenesis and patterning through a mechanism independent of direct DNA binding"[29], indicating tissue context specificity during normal development, as further supported by the evolutionary conserved roles of bHLH TFs[31].

Our lab's research focuses on the intersection of tissue engineering (TE[32]) and developmental biology (DB) that is often termed developmental engineering (DE)[33-36]. While traditional TE uses biomaterial scaffolds and signaling molecules to guide (top-down) cellular production of biological tissue substitutes, DB studies the basic science principles of tissue, organ and whole organism formation (bottom-up)[37,38]. Developmental Engineering (DE) aims, therefore, to identify, study and mimic nature's building blocks and key developmental processes to produce in vitro human tissues and organ models[36].

We came across the HAND2-HAND2-AS1 genomic locus by chance as part of an experiment detailed in this manuscript, involving human mesenchymal stem cells (hMSCs) (as model cells) that were seeded on a bioinductive porcine cardiac extracellular matrix (pcECM) scaffold. We believe accidental discoveries made through this work are of interest and possibly with wide implications. We, therefore, hope that this publication would provide an impetus for other researchers that might help elucidate the enigma involving HAND2-HAND2-AS1 regulation of MET in both tissue development, homeostasis, regeneration, and pathogenesis.

2. Materials and Methods

2.1. Decellularization and pcECM Characterization

Acellular pcECM samples (15×10×1.5 mm) were produced as we previously reported[39-41]. Briefly, native porcine left ventricular slices were sequentially immersed in alternating hyper-hypotonic solutions (1.1% and 0.7% NaCl, respectively), a trypsin (0.05%w/v)-EDTA (0.02%w/v) solution and 1% (v/v) Triton™-x-100 (in 0.1%v/v ammonium hydroxide) PBS solution. All decellularization reagents were purchased from Sigma-Aldrich (St. Louis, MO). Prior to experimentation, sliced matrices were disinfected with 70% v/v ethanol and washed with PBS containing double antibiotic-antimycotic concentration (2%v/v, Gibco™, TermoFisher Scientifc, Waltham, MA) followed by immersion in cell culture media overnight in 37 °C and 5% CO_2.

For histological analyses, three representative samples of each experimental group were fixated in fresh paraformaldehyde (4% w/v solution, PFA, Sigma-Aldrich, St. Lous, MO) for 2 hrs, and were then processed for paraffin blocks. Native tissue of similar dimensions was used as the positive control. Paraffin sections (5 μm) were processed for hematoxylin and eosin (H&E) and Masson's trichrome (MTC) stains. For immunohistochemical stains we used routine IHC staining protocols. H&E, MTC and IHC protocols used were the same as we as previously published[42] . For IHC stains we used the following primary antibodies: rabbit IgG-anti epidermal growth factor (EGF, abcam ab9695), mouse IgG anti basic fibroblast growth factor (bFGF, Mareck-Millipore, 05-118), and mouse IgG anti vascular endothelial growth factor A (VEGF, abcam, ab1316). For all staining primary antibody dilution was 1:100, antigen retrieval steps were performed in a pressure cooker for 40 min, and secondary antibody staining was performed with the Novolink polymer detection system (RE7290-K, Leica Biosystems, Germany), according to the manufacturer instructions.

2.2. hMSC culture and characterization

Human bone marrow mesenchymal stem cells (hMSCs) were commercially purchased (Poietics™, Lonza, Switzerland, PT-2501) and are guaranteed by the supplier to be $CD105^+CD166^+CD29^+CD44^+$ $CD^{14-}CD^{34-}CD45^-$ (by flow cytometry) and of being capable to differentiate down the adipogenic, chondrogenic, and osteogenic lineages when cultured in the recommended differentiation medium[43]. Cells were cultured in standard cell culture dishes using α-MEM with 10% ml FBS, 1% (v/v) antibiotic-antimycotic solution, and 1% (v/v) of 200 mM L-glutamine solution. bFGF ($5{\cdot}10^{-3}$ μg/ml) was supplemented every other day. Cells were split at 70-80% confluency at a 1:4 ratio and were used up until passage 4-5 in all experiments described herein.

To visualize the cell expression of characteristic markers we performed immunofluorescent staining on glass cover slides for representative positive and negative marker. Briefly, cells were cultured on round 18mm (0.2mm thick) cover slides in standard tissue culture plate. When reaching 70% confluence cells were fixed to the slides using ice cold methanol for 5 min followed by partial brief air drying. Subsequently slides were blocked with 3% FBS containing PBS and incubated in a humidity chamber for 30 min at RT with the following mouse anti human primary antibodies: CD90 (BD Biosciences, 555593), CD105 (BD Biosciences, 555690), CD73 (Santa Cruz Biotechnology, Inc., 32299) and CD31 used as isotype negative control (R&D systems, BBA7) all at a 1:50 dilution in 3% FBS containing PBS. Following primary antibody washes (2x) slides were incubated with a PE anti-mouse (BD Biosciences 550589, dilution 1:100) secondary antibody for 30 min RT. Subsequently slides were washed in the same serum containing wash buffer and mounted with aqueous mounting medium containing DAPI (DAPI Fluromount-G®, SouthernBiotech, Birmingham, AL). Images were acquired using the Nikon Eclipse TE2000-U equipped with a fluorescent camera at 400x magnification.

To assess the cells differentiation capacity at higher passages (passage 5), we performed cell differentiation using commercial differentiation kits. A cell solution of 1.6×10^7 cells/mL, 5×10^3 cells/mL and 1×10^4 cells/mL of hMSC were prepared with complete α-MEM media, for chondrogenesis, osteogenesis and adipogenesis differentiation, respectively (as recommended by the manufacturer protocols). 10μL droplets of cells of each cell concentrations were added to the centre

 doi:10.20944/preprints202309.1783.v1

of each well of 12-well plates and incubated in a standard 37°C 5% CO_2 incubator for 2 hrs. The α-MEM media was then replaced with the respective differentiation media and replenished every other day: StemPro® Chondrogenesis Differentiation Kit, StemPro® Osteogenesis Differentiation Kit, and StemPro® Adipogenesis Differentiation Kit (Gibco™, TermoFisher Scientifc, Waltham, MA). Staining with respective dye indicators were used after 14 days of differentiation: Alcian Blue for chondrogenesis, Alizarin Red S for osteogenesis and Oil Red O for adipogenesis (all purchased from ThermoFisher Scientific, Waltham, MA).

2.3. pcECM induced MET in hMSCs

Seeding of hMSC on the pcECM was performed on pre-cut disinfected and culture media incubated pcECM (96 well plate format) at a density of $3x10^5$ cells/cm^2 as previously published[44]. hMSC seeded pcECM constructs were cultured for 30 days. At designated time points throughout the culture mRNA was extracted (phenol and guanidine thiocyanate, qiasol™, Qiagen, Germany) from at least n=3 samples per time point (t=4, 23 and 30 days post seeding). Extracted mRNA integrity was evaluated using the 2100 Bioanalyzer (Agilent, Santa Clara, CA), and RIN values of >7 were used for subsequent steps. mRNA was reverse transcribed to cDNA using the RT² First Strand Kit (330401, Qiagen) followed by real-time qPCR analyses using two separate Qiagen RT² PCR arrays custom designed with Qiagen for specific lineage identification of endothelial and cardiomyocyte cell phenotypes (given the cardio-vascular origin of the pcECM). Lists of gene array composition and identities appear in Supplementary Tables S1-S2.

Qualitative detection of HAND2 and CD31 expression in hMSCs at the protein level in situ (on the pcECM) was performed by immunohistochemistry (IHC) and immunofluorescence (IF), respectively. HAND2 IHC was performed using a rabbit IgG anti human HAND2 (abcepta, AP17008C, 1:100) as per the protocol described above for pcECM growth factors staining with slight modifications that include antigen retrieval at pH=9, and 0.4% Triton-X-100 perforation for intracellular staining. CD31 IF was similarly performed on fixated tissue sections using the R&D systems, BBA7 mouse IgG anti human primary antibody diluted 1:50 in 3% FBS containing PBS, and a secondary PE anti-mouse (BD Biosciences 550589, dilution 1:100) for 30 min RT. Dapi was used for counter staining. Images were acquired using a fluorescent and brightfield inverted microscope (Nikon eclipse TE-2000U).

In addition, and as a more quantitative measure that avoids potential background fluorescence from the ECM, hMSCs were also harvested at designated culture time points from the pcECM and subsequently FACS analysed for quantification of CD31. For cell harvesting, hMSC seeded pcECM matrices were washed twice with 0.625 mM EDTA in PBS and transferred into 0.5 ml of Tryple 10X (ThermoFisher Scientific, Waltham, MA) in a 1.5-ml eppendorf tube. After 8 min incubation, pcECMs were removed and 0.5 ml of complete culture media (containing 10% FBS) was added in each eppendorf before centrifugation at 300 g for 5 min. All cell pellets were collected in one single tube, washed twice with cold (4°C) PBS and followed immunofluorescence staining protocol with formaldehyde against CD31 (Biolegend 303102, dilution 1:50) and PE anti-mouse (BD Biosciences 550589, dilution 1:100) for flow cytometry analysis using a BD FACS Calibur™ machine. Tissue culture plate cells served as control for this experiment. Representative results are shown out of at least n=3 samples at each time point and experimental condition as indicated.

2.4. Bioinformatic Analyses

Bioniformatic analyses for HAND2 and HAND2-AS1 expression levels was performed using several separate datasets: The National Center for Biotechnology Information (NCBI) bioproject #PRJNA280600 ("RNA sequencing of total RNA from 20 human tissues", [45]); NCBI bioproject #PRJNA270632 ("Tissue-specific circular RNA induction during human fetal development", [46]); The national institute of health (NIH) and national cancer institute (NCI) supported cancer genome atlas program (TCGA, https://www.cancer.gov/tcga); and the Genotype-Tissue Expression (GTEx) project database (dbGaP accession #phs000424.vN.pN, [47]) supported by the Common Fund of the Office of the Director of the NIH , and by NCI, NHGRI, NHLBI, NIDA, NIMH, and NINDS. Datasets from the

 doi:10.20944/preprints202309.1783.v1

NCBI bioprojects were copied from the NCBI Gene resource for HAND2 (Gene ID #9464) and HAND2-AS1 (Gene ID #79804). TCGA and GTEx data were obtained through the gene expression profiling interactive analysis 2 (GEPIA2) server[48]. All data obtained was further statistically analysed and presented using GraphPad Prism version 10.0.2 (232) for Windows (GraphPad Software, Boston, Massachusetts USA, www.graphpad.com).

2.5. CRISPR-Cas9 Knockout of HAND2-HAND2-AS1 in hMSCs

In the interest of space detailed CRISPR-Cas9 protocol and design employed appears in the supplementary information.

2.6. Statistical Analyses

Unless otherwise stated results indicate mean ± standard deviation of at least n=3 biological repetitions per sample group and time point. For statistical analyses results were first tested for normality using the Shapiro-Wilk test criteria. All results obeyed gaussian normal distribution and were therefore analysed using one-way analysis of variance (ANOVA) with Tukey's honest significant difference (HSD) post hoc correction for multiple comparisons. Adjusted p values tested are indicated by (*, $p<0.05$), (**, $p<0.01$), (***, $p<0.001$) and (****, $p<0.0001$) in the appropriate figures. (ns) indicated non-significant difference. All statistical tests and graphical results were analysed and displayed using the GraphPad Prism software version 10.0.2.

3. Results

We began our work with the decellularization of porcine hearts as we previously published[39,40] to obtain slabs of bioinductive pcECM (Figure 1). To demonstrate the preservation of ECM fibers and structure we stained paraffin sections of the native tissue (as control) and decellularized slabs with hematoxylin and eosin (H&E) and masson's trichrome (MTC) reagents. Additional immunohistochemical (IHC) stains were consequently performed for two cardio-vascular lineage specific representative growth factors (FGF2 and VEGF, respectively), and an epidermal growth factor (EGF) serving as negative control (Figure 1 as indicated). These stains confirmed retention of cardio-vascular growth factor pockets within the pcECM following decellularization, which is in accordance with previously described mechanisms of ECM biological composition and function[42,49-51].

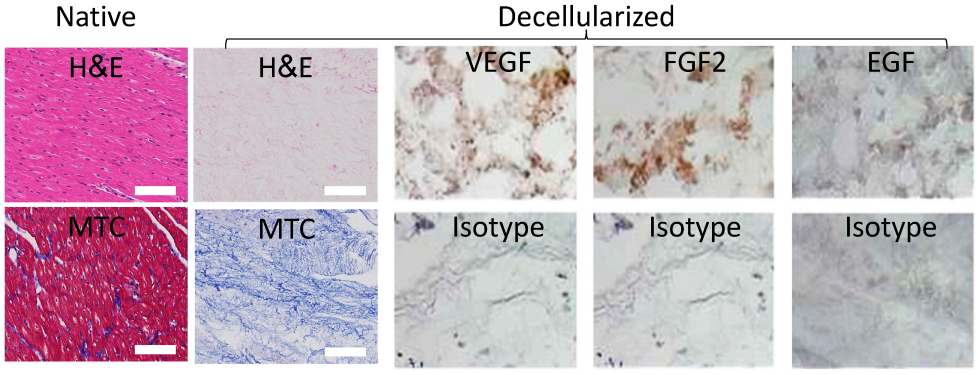

Figure 1. Decellularized porcine cardiac extracellular matrix (pcECM) is acellular and preserves cardio-vascular tissue specific ultrastructure and bioactive growth factors. Decellularized pcECM was paraffin cross sectioned and compared to native porcine left ventricular tissue using hematoxylin and eosin (H&E) and Masson's tri-chrome (MTC) stains, as indicated. Sequential paraffin cross sections of the pcECM were also immunohistochemically (IHC) stained, as indicated, for two representative cardio-vascular related growth factors: basic fibroblast growth factor (bFGF) and vascular endothelial growth factor A (VEGF), respectively. IHC staining for epidermal growth factor (EGF) is also presented as control, along with the isotype staining for each case. Scale bars: 100μm. Microscope

Preprints (www.preprints.org) | NOT PEER-REVIEWED | Posted: 26 September 2023 doi:10.20944/preprints202309.1783.v1

magnifications: 200x. Representative images are presented out of at least n=3 biological samples and n=2 IHC / histological section stains tested for each group.

Prior to repopulating our pcECM scaffold with hMSCs (commercially purchased from Lonza, Switzerland) we performed characterization of cell morphology, marker expression profile and differentiation potency (Figure 2). These analyses demonstrated tissue-culture plastic adherence, characteristic spindle shaped morphology, consensus marker expression ($CD73^{+}CD90^{+}CD105^{+}CD31^{-}$), and multipotency following standard protocols for adipose, bone and cartilage-like cell differentiation. Of note was the absence of CD31 expression by the hMSCs (used as iso-type negative control), which suggested the lack of endothelial commitment by the cells used.

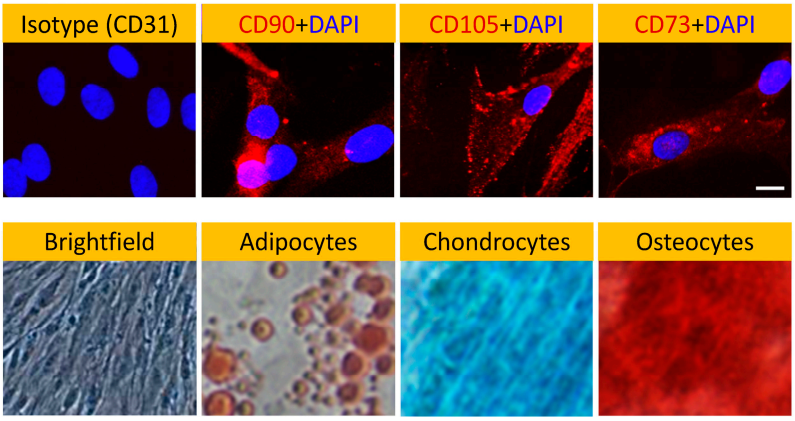

Figure 2. Human mesenchymal stem cells (hMSCs) characterization. Negative ($CD31^{-}$, isotype control) and positive ($CD90^{+}CD105^{+}CD73^{+}$, as indicated) marker stains for bone marrow hMSCs (Lonza, Switzerland) show consensus marker expression. Cellular morphology even at passage 5 remained characteristic of hMSCs as indicated by brightfield phase contrast microscopy. Furthermore, the cells differentiation potential appeared to be conserved at that passage as well as shown for hMSC derived differentiated adipocytes- (oil red), chondrocytes- (Alcian blue) and osteocytes- (Alizarin red S) like cells, as indicated. Brightfield image shows untreated hMSC control morphology. Magnifications: Brightfield–100x; Fluorescent images–200x; Differentiation images: 40x.

At distinct time points (t=3, 23 and 30 days) during the culture we isolated the hMSCs (through trypsinization) and obtained their mRNA. To identify possible induction pathways that may be triggered by the pcECM, the mRNA was then subject to reverse transcribed quantitative (realtime) polymerase chain reaction (RT-qPCR) arrays (Supplementary information online and Supplementary Tables S1 and S2) for cardiac and endothelial related genes. Analyzing these data, we observed two interesting and sequential phenomena. At the initial time points following seeding, the mRNA levels of HAND2 were significantly up regulated (~2400 fold, relative to standard tissue culture plate expression levels, Supplementary Table S3). This upregulation was also observed in repeated experiments at the protein level on day 4 of culture using IHC cross sectional histological staining specifically for HAND2 (Figure 3). While the mRNA level of HAND2 subsided to lower values at later time points (Supplementary Table S3), the HAND2 protein level remained persistent at least until day 10 of culture (data not shown). This phenomenon preceded and was concomitant to upregulation of endothelial related genes, including PECAM1 (CD31), for which the hMSCs were originally negative before seeding (Supplementary Table S3). Intrigued by these results, we further performed protein level evaluation of CD31 expression by the seeded hMSCs revealing a gradual increase in its presence throughout the 30 days of culture as evidenced by both flow cytometry and by immunofluorescent stains (Figure 3). Collectively, these results suggested that the pcECM induced an MET process in the seeded hMSCs driving their partial commitment towards an endothelial (simple squamous epithelium) phenotype.

Preprints (www.preprints.org) | NOT PEER-REVIEWED | Posted: 26 September 2023 doi:10.20944/preprints202309.1783.v1

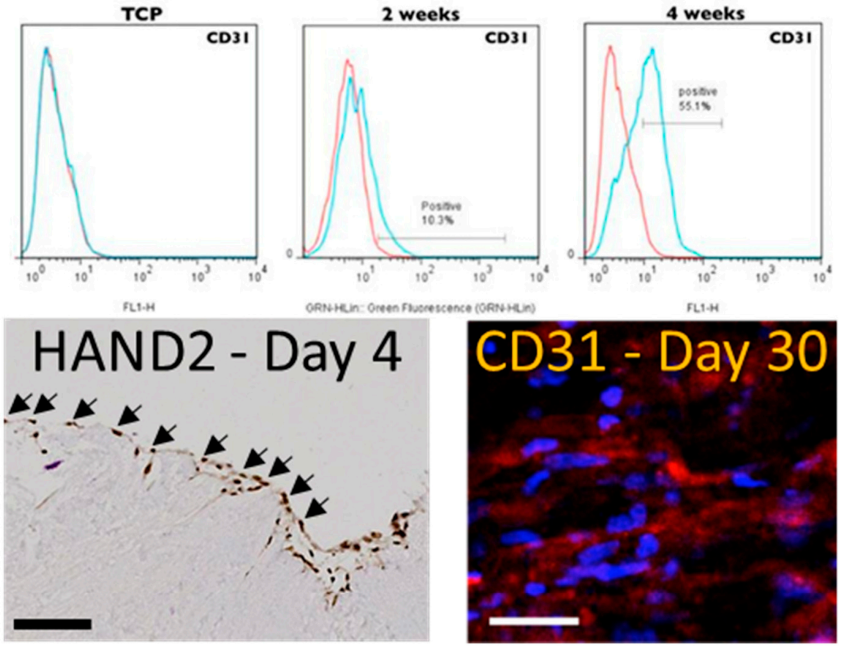

Figure 3. pcECM induced early HAND2 expression followed by gradual MET towards an endothelial phenotype. Three to four days after seeding, hMSCs on pcECM expressed high levels of HAND2 at the mRNA (Supplementary Table T3) and protein levels (HAND2 – Day 4 nuclei localization, IHC bottom left image as indicated). This was accompanied by hMSCs exhibiting an unusual squamous monolayer epithelial-like morphology (arrows in HAND2 IHC image) and was followed by a gradual increase in the expression of endothelial cell markers through long-term (up to 30 days) cultures (Supplementary Table T3). Protein level expression of endothelial markers is demonstrated by CD31/PECAM^{+} presence in both trypsinized hMSCs (using fluorescent activated cell sorting, FACS, at two and four weeks after seeding, top row) and in situ immunofluorescence imaging (CD31 – Day 30 as indicated). Scale bars: IHC HAND2 stain: 500μm. CD31 IF stain: 100μm.

Interestingly, HAND2 has only two exons (Chr. 4q34.1, Genecards database[52]) but its promoter region and first exon partially overlap an associated antisense long noncoding RNA (lncRNA, HAND2-AS1)—implicated in alleviating numerous human pathologies reviewed in[53,54]. We performed bioinformatic analyses of HAND2 and HAND2-AS1 expression data using known human sequencing databases for adult and fetal normal expression as well as pathological expression levels in various cancers. These bioinformatic data correlation and analyses suggested that in normal adult tissues (Figure 4a,b), during fetal development (Figure 4a-b insets), and also during cancer progression (Figure 4c) HAND2 and HAND2-AS1 expression profiles seemed to correlate (Figure 4d) and obey similar trends. In adults, high HAND2-HAND2-AS1 expression levels appear either in tissues that contain neural crest lineage cells and that appear very early in embryonic organogenesis and development (such as the adrenal glands and the heart) or in tissues that are associated with pregnancy (i.e., the endometrium, ovary, and placenta). Other renewable tissues that had high HAND2-HAND2-AS1 expression levels during development (e.g., stomach, kidney, and intestine) seem to lower their expression to a more moderate level in adulthood. However, the HAND-2 and HAND2-AS1 tissue level expression during homeostasis seems to be highly maintained, as protrusion/imbalance at the tissue level is associated with many different cancer types (Figure 4c). Among these cancer types shown, are two major categories – those with downregulation of HAND2 and HAND2-AS1 expression relative to healthy tissue controls (most cancers analyzed) and those with HAND2 and HAND2-AS1 upregulation (specific for pancreatic adenocarcinoma, PAAD; and for pheochromocytoma and paraganglioma, PCPG).

Preprints (www.preprints.org) | NOT PEER-REVIEWED | Posted: 26 September 2023 doi:10.20944/preprints202309.1783.v1

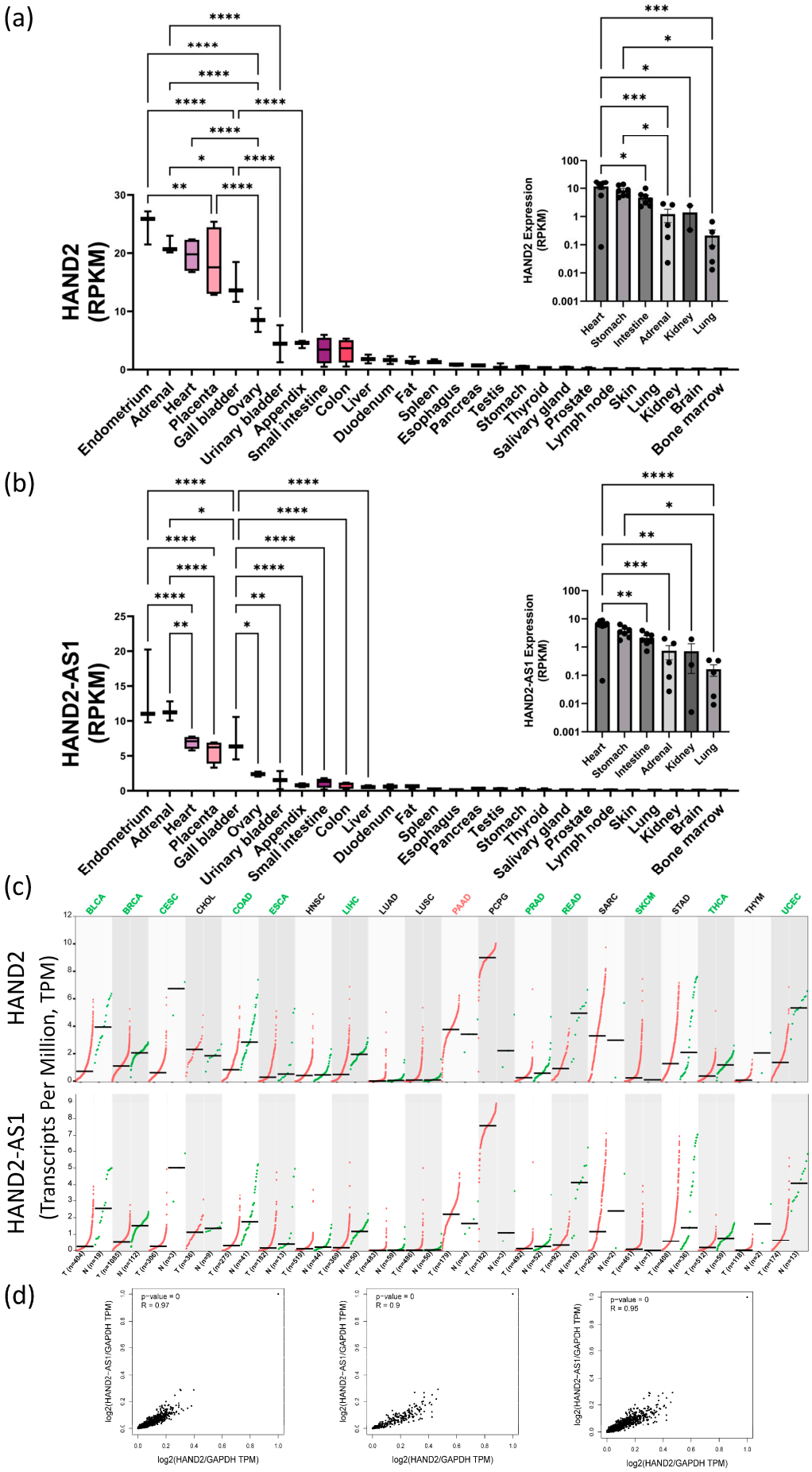

 doi:10.20944/preprints202309.1783.v1

Figure 4. Bioinformatic analyses of HAND2 and its associated lncRNA HAND2-AS1 expression patterns in adult, embryonic and pathological tissues Bioinformatic analyses of HAND2 (NCBI Gene accession: 9464, a) and HAND2-AS1 (NCBI Gene accession: 79804, b) expression in adult human tissues (reads per kilobase per million reads, RPKM) based on the national center for biotechnology information (NCBI) bioproject #PRJNA280600 ("RNA sequencing of total RNA from 20 human tissues", [45]). Insets in (a) and (b) show corresponding HAND2 and HAND2-AS1 embryonic expression, respectively, at sampled tissues between weeks 10 to 20 of human gestation as sourced from the NCBI bioproject #PRJNA270632 ("Tissue-specific circular RNA induction during human fetal development", [46]); Expression levels of HAND2 and HAND2-AS1 (RPKM, as indicated) in a collection of cancer samples (red dots), relative to neighboring normal tissue samples (green dots) are shown side by side for various cancer types abbreviated as follows: BLCA– Bladder Urothelial Carcinoma; BRCA– Breast invasive carcinoma; CESC– Cervical squamous cell carcinoma and endocervical adenocarcinoma; CHOL– Cholangiocarcinoma; COAD– Colon adenocarcinoma; ESCA– Esophageal carcinoma; HNSC– Head and Neck squamous cell carcinoma; LIHC– Liver hepatocellular carcinoma; LUAD– Lung adenocarcinoma; LUSC– Lung squamous cell carcinoma; PAAD– Pancreatic adenocarcinoma; PCPG– Pheochromocytoma and Paraganglioma; PRAD– Prostate adenocarcinoma; READ– Rectum adenocarcinoma; SARC– Sarcoma; SKCM– Skin Cutaneous Melanoma; STAD– Stomach adenocarcinoma; THCA– Thyroid carcinoma; THYM– Thymoma; UCEC– Uterine Corpus Endometrial Carcinoma. Cancer data was obtained from the national institute of health (NIH) and national cancer institute (NCI) supported cancer genome atlas program (TCGA); and from the Genotype-Tissue Expression (GTEx) project databases (data sources appear in the materials and methods section). Correlation between HAND2 and HAND2-AS1 expression levels in normal tissues (d, left), tumor tissues (d, middle), and combined normal and tumor tissues (d, right), combining both the TCGA and GTEx data sets.

Intrigued by our bioinformatic analyses results, we performed hMSCs knockout (KO) of both HAND2 first exon and HAND2-AS1 regulatory/promoter genomic region (Figure 5a, indicated by purple rectangle) using CRISPR-Cas9 (Supplementary Fig. S1). Our initial thought was that given the tissue specificity and the small (only two exons) scale of this gene, knocking it down might not be detrimental to hMSCs. Clearly, using such KO hMSCs (HAND2-HAND2-AS1^{null}) would enable testing the apparent regulation of the HAND2/HAND2-AS1 gene products on pcECM induced hMSC-MET towards endothelial phenotypes.

Surprisingly, while the gene editing was successful in obtaining double 'mutant' KO hMSC cells (Figure. 5b, mix MUT lane, Supplementary Figure S2), the HAND2/HAND2-AS1 gene products seems to be vital at least at a basal (low) expression level for hMSC proliferation and function. In fact, within the transfected cell populations appearing on the same plate and culture conditions (Figure 5c) two cell morphologies became apparent following the CRISPR-Cas9 editing. One rare morphology (3 discrete colonies) was identical to wildtype (WT) hMSC. These cells continued to proliferate, and were capable of subculturing, i.e., localized short and low volume trypsinization enabled to selectively lift and propagate them in other tissue culture dishes. Once propagated these colonies' clones (marked as clone 1-clone 3, lanes 2-4, Figure 5b) exhibited a heterozygous HAND2 PCR product containing both mutant/KO phenotype of 260bp (short/edited) and a 976 bp (WT) PCR product bands on agarose gel electrophoresis. Most of the cell population however, displayed a senescent-like hypertrophic and cell–cycle arrested morphological phenotype (Figure 5C, MUT marked morphologies compared to WT/colony standard morphology). These cells did not organize into colonies and remained hypertrophic and quiescent/senescent for at least 3 weeks on plate. The mRNA of these cell types was harvested (labeled mix MUT in Figure 5b) and their PCR product displayed a homozygous short HAND2 band. This band was further sanger sequenced to determine the actual deletion sequence is correct (as designed, Supplementary Figure S2). Given the paucity of this cell type and the lack of its proliferation, we were unable to perform additional characterization.

Preprints (www.preprints.org) | NOT PEER-REVIEWED | Posted: 26 September 2023 doi:10.20944/preprints202309.1783.v1

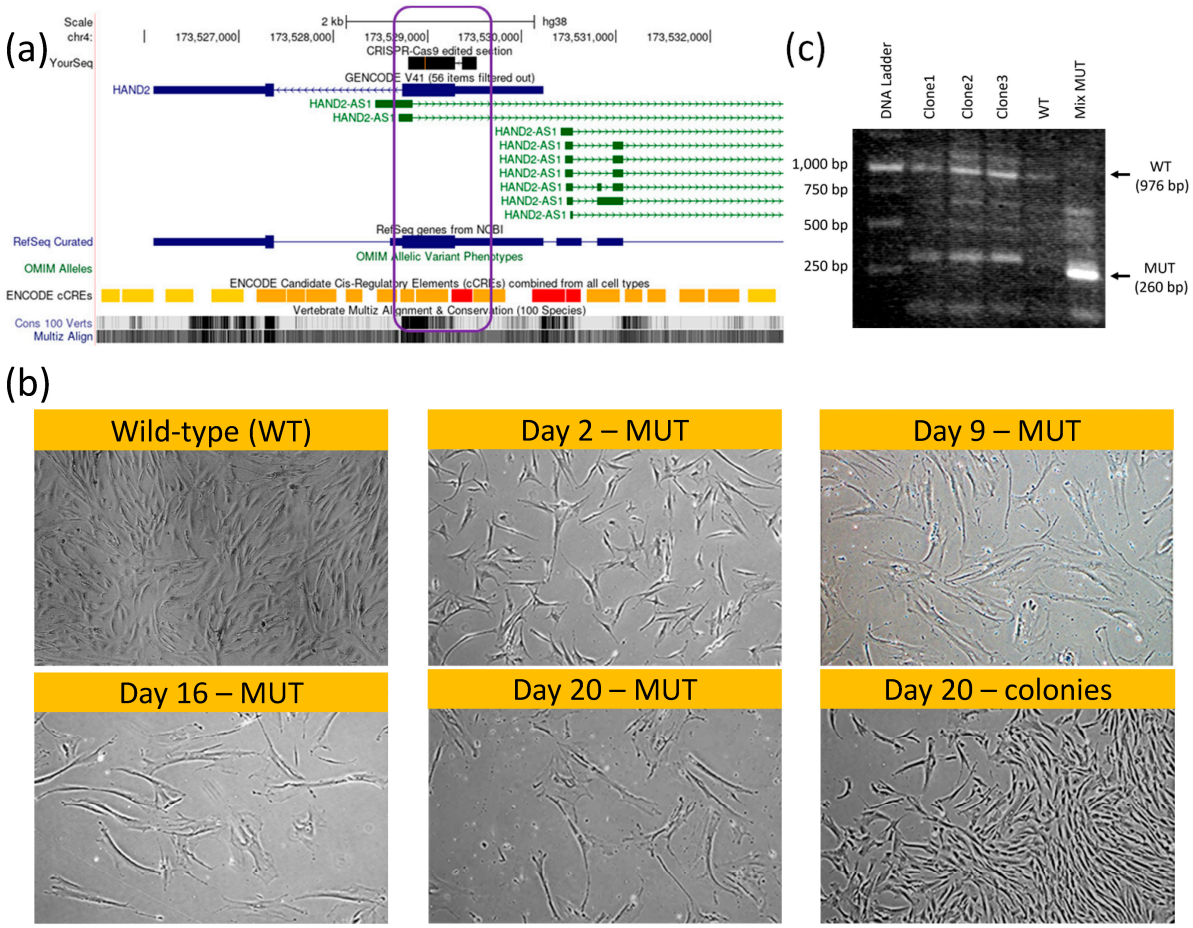

Figure 5. HAND2/HAND2-AS1 locus knockout (KO) hMSCs using CRISPR-Cas9 genomic editing. Genome view of HAND2 (sense strand, blue) and HAND2-AS1 isoforms (antisense strand, green) sharing a common promoter region (red ENCODE region, a), in which permanent KO (b, CRISPR–Cas9 black sequence top lane; KO region is graphically displayed by purple rectangle; KO vector map is provided in Supplementary Figure S1) led to a hMSC senescent morphology (b, MUT-marked images show time progression of proliferation-arrest and hypertrophy within the same wells, without passaging) compared to wild-type (WT) and to heterozygous cells that managed to form characteristic hMSC colonies (b, as indicated). Given the scarcity of full MUT cells (non-dividing) we compared HAND2 PCR products using gel electrophoresis (c) for the original (WT, untreated) and total gene-edited plates (mixed MUT) comprising mostly HAND2$^{-/-}$ senescent cells. Colony clones (clone 1–clone 3) displayed a mixed WT-MUT band signature suggesting heterozygosity to the CRISPR-Cas9 editing. Mixed MUT band comprising mostly HAND2$^{-/-}$ senescent cells displayed a shorter bright mutant 260 bp band. Sanger sequencing of that mutant (MUT) band confirmed deletions compared to the original sequence as per vector design (Supplementary Figure S2).

Nevertheless, and taken together with the results of HAND2 involvement in MET induction, these observations further suggest distinct concentration-dependent HAND2/HAND2-AS1 control of cell phenotype. That is, no HAND2/HAND2-AS1 expression (complete absence) causes senescence (or at minimum cell cycle arrest and cellular hypertrophy), basal low–intermediate expression is critical to maintain the mesenchymal phenotype, and high expression levels may induce MET toward epithelial/endothelial phenotypes. To the best of our knowledge, this finding is new, may be of potential interest to the readership of this journal, and merits further elucidation.

4. Discussion

The bioactivity of the pcECM scaffold material *in vitro*[41,44,55,56] and *in vivo*[42,57] (REFs) has been thoroughly described by our group and others including induction of cardiac commitment in human

 doi:10.20944/preprints202309.1783.v1

induced pluripotent stem cells (hiPSCs) in the absence of induction media[55], stimulation of neo-tissue formation[41] (REF), and modulation of host immunity resulting in recruitment of host progenitor cells that assist in cardiac regeneration even after scarring in rat myocardial infarction models[42,57]. This is in accordance with an established body of evidence on the biological activity, tissue specificity, and induction capacity of decellularized ECM based materials[49-51]. Thus, in the absence of an immune response (in a completely in vitro setting) the gradual nature of the effect observed may be attributes to dependency on ECM remodelling by the cells, which help release localized high concentration of growth factors retained within the decellularized composite ECM. Such high localized concentrations may be a strong driving force in selectively directing stem cell fate decisions and differentiation states in a tissue specific manner which is dependent on the relative abundance and composition of tissue resident growth factors.

Regardless of the actual activation molecular pathway involved, our findings clearly indicate transient activation of HAND2 in hMSCs seeded on the pcECM which preceded their MET towards endothelial phenotypes. Our bioinformatic analyses further revealed that HAND2 and HAND2-AS1 expression levels are tightly correlated (Pearson coefficient > 0.90) across many different tissues both during embryonic organogenesis (between weeks 10 and 20), as well as in adult normal and pathologic conditions. This tight regulation suggests that HAND2-HAND2-AS1 may be involved in a centrally conserved and important regulatory mechanism, the nature of which is currently unknown. Our findings suggest that this regulatory pathway results in highly active HAND2 expression during organogenesis. This HAND2 expression is subsequently reduced in most adult tissues to basal medium-low levels, except for the endometrium, heart, adrenal and placenta, where HAND2 expression levels remain high even in adulthood. A common denominator to these high HAND2 expressing tissues may be the fact that they are all critical for embryonic support and pregnancy related hormonal regulation. In addition, human protein level analyses[58] for HAND2 suggest its constant low-medium level expression, in many tissues, beyond those that were identified by our sequencing data analyses, and at a histologically verified manner.

Taken together, we suggest that this HAND2-HAND2-AS1 regulatory pathway may represent a fine-tuning mechanism regulating plasticity in a spectrum/axis comprising senescence-like phenotype (complete absence of HAND2/HAND2-AS1 expression), maintenance of mesodermal/mesenchyme stemness/proliferation capacity (at basal expression levels), and MET (at high levels). This suggested mechanism is further supported by the similarity of adult hMSCs to neural crest cells, that are considered the fourth germ layer, the literary evidence suggesting HAND2/HAND2-AS1 role as a regulator of many cancer types, and the critical role of MET in cancer progression and metastasis, as outlined below.

At the molecular level, regulation of adult endometrial HAND2 function is the most substantiated. There it is induced by upstream progesterone (P4)-Indian hedgehog (IHH) signaling during menstrual cycles and initiates downstream MET (also termed decidualization[59])—a key requirement for blastocyst receptivity during implantation[60]. In wider adult-tissue pathological contexts (type 2/3 MET), however, HAND2 is associated with endometriosis induction (upregulating proinflammatory IL15 expression[61,62]), right ventricle protection from pressure overload damage[26], familial dilated cardiomyopathy[63], onset of mesothelioma malignancies[30] and obesity (regulated by glucocorticoid signaling)[64]. HAND2 is also silenced in colorectal cancer (via hypermethylation correlated with poor prognosis) and has been identified as an epigenetic driver gene and a potential tumor suppressor (via MAPK/ERK signaling)[65]. Interestingly, HAND2 and its associated lncRNA, HAND2-AS1, were implicated in alleviating numerous human pathologies reviewed in[53,54]. It is reasonable that HAND-AS1-induced MET can be a shared underlying mechanism initiating atherosclerosis prevention[66,67], impairment of fibroblast activation in rheumatoid arthritis[68], and inhibition of glioma[69], prostate[70], ovarian[71,72], gastric[73], bladder[74], cervical[75,76], breast[77], and pancreatic[78] cancer progression with mixed reports in liver cancer[79-81].

To date, studying HAND2 function in vitro focused on primary human cardiac mesenchymal stromal cells (cMSCs), where its ability to induce MET toward an endothelial (simple squamous epithelium) state in a senescent selective manner (corelated to CD90 pre-expression) was

demonstrated[18]. Other studies using bone marrow human mesenchymal stem/stromal cells (hMSCs) showed that IHH signaling affects cellular senescence through modulation of ROS/mTOR/4EBP1 and p70S6K1/2 signaling—a key molecular pathway in aging[82]. While HAND2 was not directly explored in the latter study, senescence dependency on IHH signaling may also be relevant to HAND2 activation (as occurring in the endometrium); this merits further elucidation using adequate cell and tissue models.

Collectively, HAND2 and HAND2-AS1 are, therefore, suggested herein as common downstream regulators of MET during embryonic cardiac tissue (and also digit development), in adult heart, endometrium, renewable epithelial and adipose tissues, and within wider tissue contexts of senescence and related pathologies. It is also reasonable that regulation of MET (which results in a wide spectrum of commitment levels) would occur in a manner which is proportional to expression level. Indeed, several different HAND2 activators (cardiac Notch, endometrial progesterone-IHH, and adipose glucocorticoid signaling) along with its lncRNA (HAND2-AS1) epigenetic regulation pinpoint the HAND2-HAND2-AS1 loci as a possible local integrator and driver of MET in tissue development, renewal and senescence. The fascinating MET roles of HAND2 and HAND2-AS1 within such diverse biological contexts remain to be elucidated and to this end necessitate the development of appropriate inflammation-free human 3D cell and tissue models.

Our suggested mechanism has far-reaching implications for both developmental biology, regenerative medicine, tissue engineering, and as a possibly common treatment target for many related pathologies. Nevertheless, further investigations and efforts are required to verify and corroborate our findings and suggested mechanism, better understand this regulatory pathway, identify a more controlled environment that can selectively induce and inhibit this pathway, and ultimately understand the molecular players involved. We also suggest that targeting this pathway may represent a promising new therapeutic approach for a wide range of diseases, including cancer, degenerative disorders, and aging.

Supplementary Materials: The following supporting information can be downloaded at the website of this paper posted on Preprints.org.

Author Contributions: Conceptualization, Udi Sarig; Formal analysis, Rachel Vazana-Netzarim, Hod Bruck and Naama Danino; Investigation, Rachel Vazana-Netzarim; Methodology, Rachel Vazana-Netzarim and Shachar Sofer; Supervision, Udi Sarig; Validation, Rachel Vazana-Netzarim and Yishay Elmalem; Writing – original draft, Udi Sarig; Writing – review & editing, Rachel Vazana-Netzarim, Shachar Sofer, Hod Bruck, Naama Danino and Udi Sarig.

Funding: This research was supported by the Ministry of Innovation, Science & Technology, Israel (grant number: 0004628), and by the Singapore National Research Foundation (under the CREATE program).

Acknowledgement: The authors would like to acknowledge the contribution of Evelyne Bao-Vi Nguyen, Priyadarshini S Mhaisalkar, and Yu Wei Ping for their assistance.

Institutional Review Board Statement: Not applicable.

Informed Consent Statement: Not applicable.

Data Availability Statement: The data presented in this study are available on request from the corresponding author.

Conflicts of Interest: The authors declare no conflict of interest.

References

1. Yang, J. et al. Guidelines and definitions for research on epithelial-mesenchymal transition. *Nat Rev Mol Cell Biol* **21**, 341-352 (2020). https://doi.org:10.1038/s41580-020-0237-9
2. Santos, F., Moreira, C., Nobrega-Pereira, S. & Bernardes de Jesus, B. New Insights into the Role of Epithelial(-)Mesenchymal Transition during Aging. *Int J Mol Sci* **20** (2019). https://doi.org:10.3390/ijms20040891
3. Chung, S. & Andrew, D. J. The formation of epithelial tubes. *J Cell Sci* **121**, 3501-3504 (2008). https://doi.org:10.1242/jcs.037887

4. Thiery, J. P., Acloque, H., Huang, R. Y. & Nieto, M. A. Epithelial-mesenchymal transitions in development and disease. *Cell* **139**, 871-890 (2009). https://doi.org:10.1016/j.cell.2009.11.007
5. Nieto, M. A. Epithelial plasticity: a common theme in embryonic and cancer cells. *Science* **342**, 1234850 (2013). https://doi.org:10.1126/science.1234850
6. Nieto, M. A. Are You Interested or Afraid of Working on EMT? *Methods Mol Biol* **2179**, 19-28 (2021). https://doi.org:10.1007/978-1-0716-0779-4_4
7. Gilbert, S. F. & Barresi, M. J. F. *Developmental biology*. 12 edn, (Oxford University Press, 2020).
8. Amack, J. D. Cellular dynamics of EMT: lessons from live in vivo imaging of embryonic development. *Cell Commun Signal* **19**, 79 (2021). https://doi.org:10.1186/s12964-021-00761-8
9. Pei, D., Shu, X., Gassama-Diagne, A. & Thiery, J. P. Mesenchymal-epithelial transition in development and reprogramming. *Nat Cell Biol* **21**, 44-53 (2019). https://doi.org:10.1038/s41556-018-0195-z
10. Gouignard, N., Andrieu, C. & Theveneau, E. Neural crest delamination and migration: Looking forward to the next 150 years. *Genesis* **56**, e23107 (2018). https://doi.org:10.1002/dvg.23107
11. Kalcheim, C. in *Neural Crest Cells: Methods and Protocols* (eds Quenten Schwarz & Sophie Wiszniak) 1-19 (Springer New York, 2019).
12. Escot, S. et al. Disruption of CXCR4 signaling in pharyngeal neural crest cells causes DiGeorge syndrome-like malformations. *Development* **143**, 582-588 (2016). https://doi.org:10.1242/dev.126573
13. Cortes, C., Francou, A., De Bono, C. & Kelly, R. G. Epithelial Properties of the Second Heart Field. *Circ Res* **122**, 142-154 (2018). https://doi.org:10.1161/CIRCRESAHA.117.310838
14. Kim, J. H. & Choi, M. H. Embryonic Development and Adult Regeneration of the Adrenal Gland. *Endocrinol Metab (Seoul)* **35**, 765-773 (2020). https://doi.org:10.3803/EnM.2020.403
15. Marconi, G. D. et al. Epithelial-Mesenchymal Transition (EMT): The Type-2 EMT in Wound Healing, Tissue Regeneration and Organ Fibrosis. *Cells* **10** (2021). https://doi.org:10.3390/cells10071587
16. Jia, D. et al. Towards decoding the coupled decision-making of metabolism and epithelial-to-mesenchymal transition in cancer. *Br J Cancer* **124**, 1902-1911 (2021). https://doi.org:10.1038/s41416-021-01385-y
17. Kishi, S., Bayliss, P. E. & Hanai, J. A prospective epigenetic paradigm between cellular senescence and epithelial-mesenchymal transition in organismal development and aging. *Transl Res* **165**, 241-249 (2015). https://doi.org:10.1016/j.trsl.2014.05.007
18. Martini, H. et al. Aging induces cardiac mesenchymal stromal cell senescence and promotes endothelial cell fate of the CD90 + subset. *Aging Cell* **18**, e13015 (2019). https://doi.org:10.1111/acel.13015
19. Wang, M. et al. SIRT1 upregulation promotes epithelial-mesenchymal transition by inducing senescence escape in endometriosis. *Sci Rep* **12**, 12302 (2022). https://doi.org:10.1038/s41598-022-16629-x
20. Aach, J., Lunshof, J., Iyer, E. & Church, G. M. Addressing the ethical issues raised by synthetic human entities with embryo-like features. *Elife* **6** (2017). https://doi.org:10.7554/eLife.20674
21. Hahn, S. et al. Organoid-based epithelial to mesenchymal transition (OEMT) model: from an intestinal fibrosis perspective. *Sci Rep* **7**, 2435 (2017). https://doi.org:10.1038/s41598-017-02190-5
22. Fatehullah, A., Tan, S. H. & Barker, N. Organoids as an in vitro model of human development and disease. *Nat Cell Biol* **18**, 246-254 (2016). https://doi.org:10.1038/ncb3312
23. Campbell, K. & Theveneau, E. e. *The Epithelial-to Mesenchymal Transition: Methods and Protocols*. (Springer US, 2021).
24. Firulli, B. A., Hadzic, D. B., McDaid, J. R. & Firulli, A. B. The basic helix-loop-helix transcription factors dHAND and eHAND exhibit dimerization characteristics that suggest complex regulation of function. *J Biol Chem* **275**, 33567-33573 (2000). https://doi.org:10.1074/jbc.M005888200
25. Srivastava, D. et al. Regulation of cardiac mesodermal and neural crest development by the bHLH transcription factor, dHAND. *Nat Genet* **16**, 154-160 (1997). https://doi.org:10.1038/ng0697-154
26. Videira, R. F. et al. The adult heart requires baseline expression of the transcription factor Hand2 to withstand RV pressure overload. *Cardiovasc Res* (2021). https://doi.org:10.1093/cvr/cvab299
27. VanDusen, N. J. et al. Hand2 is an essential regulator for two Notch-dependent functions within the embryonic endocardium. *Cell Rep* **9**, 2071-2083 (2014). https://doi.org:10.1016/j.celrep.2014.11.021
28. Barnes, R. M. et al. Hand2 loss-of-function in Hand1-expressing cells reveals distinct roles in epicardial and coronary vessel development. *Circ Res* **108**, 940-949 (2011). https://doi.org:10.1161/CIRCRESAHA.110.233171
29. McFadden, D. G., McAnally, J., Richardson, J. A., Charite, J. & Olson, E. N. Misexpression of dHAND induces ectopic digits in the developing limb bud in the absence of direct DNA binding. *Development* **129**, 3077-3088 (2002). https://doi.org:10.1242/dev.129.13.3077
30. Prummel, K. D. et al. Hand2 delineates mesothelium progenitors and is reactivated in mesothelioma. *Nat Commun* **13**, 1677 (2022). https://doi.org:10.1038/s41467-022-29311-7
31. de Martin, X., Sodaei, R. & Santpere, G. Mechanisms of Binding Specificity among bHLH Transcription Factors. *Int J Mol Sci* **22** (2021). https://doi.org:10.3390/ijms22179150
32. Langer, R. & Vacanti, J. P. Tissue engineering. *Science* **260**, 920-926 (1993). https://doi.org:10.1126/science.8493529

33. Lenas, P. & Ikonomou, L. Developmental engineering: design of clinically efficacious bioartificial tissues through developmental and systems biology. *Sci China Life Sci* **61**, 978-981 (2018). https://doi.org:10.1007/s11427-017-9255-3
34. Lenas, P., Moos, M. & Luyten, F. P. Developmental engineering: a new paradigm for the design and manufacturing of cell-based products. Part II: from genes to networks: tissue engineering from the viewpoint of systems biology and network science. *Tissue Eng Part B Rev* **15**, 395-422 (2009). https://doi.org:10.1089/ten.TEB.2009.0461
35. Lenas, P., Moos, M. & Luyten, F. P. Developmental engineering: a new paradigm for the design and manufacturing of cell-based products. Part I: from three-dimensional cell growth to biomimetics of in vivo development. *Tissue Eng Part B Rev* **15**, 381-394 (2009). https://doi.org:10.1089/ten.TEB.2008.0575
36. Zarkesh, I. et al. Synthetic developmental biology: Engineering approaches to guide multicellular organization. *Stem Cell Reports* **17**, 715-733 (2022). https://doi.org:10.1016/j.stemcr.2022.02.004
37. Zohorsky, K. & Mequanint, K. Designing Biomaterials to Modulate Notch Signaling in Tissue Engineering and Regenerative Medicine. *Tissue Eng Part B Rev* **27**, 383-410 (2021). https://doi.org:10.1089/ten.TEB.2020.0182
38. Ho, C. & Morsut, L. Novel synthetic biology approaches for developmental systems. *Stem Cell Reports* **16**, 1051-1064 (2021). https://doi.org:10.1016/j.stemcr.2021.04.007
39. Eitan, Y., Sarig, U., Dahan, N. & Machluf, M. Acellular cardiac extracellular matrix as a scaffold for tissue engineering: in vitro cell support, remodeling, and biocompatibility. *Tissue Eng Part C Methods* **16**, 671-683 (2010). https://doi.org:10.1089/ten.TEC.2009.0111
40. Sarig, U. et al. Thick acellular heart extracellular matrix with inherent vasculature: a potential platform for myocardial tissue regeneration. *Tissue Eng Part A* **18**, 2125-2137 (2012). https://doi.org:10.1089/ten.TEA.2011.0586
41. Sarig, U. et al. Biological and mechanical interplay at the Macro- and Microscales Modulates the Cell-Niche Fate. *Sci Rep* **8**, 3937 (2018). https://doi.org:10.1038/s41598-018-21860-6
42. Sarig, U. et al. Natural myocardial ECM patch drives cardiac progenitor based restoration even after scarring. *Acta Biomater* **44**, 209-220 (2016). https://doi.org:10.1016/j.actbio.2016.08.031
43. Lonza. *hMSC - Human Mesenchymal Stem Cells*, <https://bioscience.lonza.com/lonza_bs/CH/en/Primary-and-Stem-Cells/p/00000000000186706/hMSC---Human-Mesenchymal-Stem-Cells> (2023).
44. Sarig, U. et al. Pushing the envelope in tissue engineering: ex vivo production of thick vascularized cardiac extracellular matrix constructs. *Tissue Eng Part A* **21**, 1507-1519 (2015). https://doi.org:10.1089/ten.TEA.2014.0477
45. Duff, M. O. et al. Genome-wide identification of zero nucleotide recursive splicing in Drosophila. *Nature* **521**, 376-379 (2015). https://doi.org:10.1038/nature14475
46. Szabo, L. et al. Statistically based splicing detection reveals neural enrichment and tissue-specific induction of circular RNA during human fetal development. *Genome Biol* **16**, 126 (2015). https://doi.org:10.1186/s13059-015-0690-5
47. dbGAP. *Common Fund (CF) Genotype-Tissue Expression Project (GTEx) (dbGaP Study Accession: phs000424.v9.p2)*, <https://www.ncbi.nlm.nih.gov/projects/gap/cgi-bin/study.cgi?study_id=phs000424.v9.p2> (2023).
48. Tang, Z. et al. GEPIA: a web server for cancer and normal gene expression profiling and interactive analyses. *Nucleic Acids Res* **45**, W98-W102 (2017). https://doi.org:10.1093/nar/gkx247
49. Badylak, S. F. The extracellular matrix as a biologic scaffold material. *Biomaterials* **28**, 3587-3593 (2007). https://doi.org:10.1016/j.biomaterials.2007.04.043
50. Mewhort, H. E. et al. Epicardial infarct repair with bioinductive extracellular matrix promotes vasculogenesis and myocardial recovery. *J Heart Lung Transplant* **35**, 661-670 (2016). https://doi.org:10.1016/j.healun.2016.01.012
51. Saldin, L. T., Cramer, M. C., Velankar, S. S., White, L. J. & Badylak, S. F. Extracellular matrix hydrogels from decellularized tissues: Structure and function. *Acta Biomater* **49**, 1-15 (2017). https://doi.org:10.1016/j.actbio.2016.11.068
52. Safran, M. et al. in *Practical Guide to Life Science Databases* Ch. Chapter 2, 27-56 (2021).
53. Gu, X., Zheng, Q., Chu, Q. & Zhu, H. HAND2-AS1: A functional cancer-related long non-coding RNA. *Biomed Pharmacother* **137**, 111317 (2021). https://doi.org:10.1016/j.biopha.2021.111317
54. Da, C. M. et al. Role of HAND2-AS1 in human tumors. *Clin Chim Acta* **511**, 189-197 (2020). https://doi.org:10.1016/j.cca.2020.10.020
55. Krishnamoorthi, M. K. et al. Robust Fabrication of Composite 3D Scaffolds with Tissue-Specific Bioactivity: A Proof-of-Concept Study. *ACS Appl Bio Mater* **3**, 4974-4986 (2020). https://doi.org:10.1021/acsabm.0c00310
56. Chi Ting Au-Yeung, G. et al. Restoring the biophysical properties of decellularized patches through recellularization. *Biomater Sci* **5**, 1183-1194 (2017). https://doi.org:10.1039/c7bm00208d
57. Efraim, Y. et al. Biohybrid cardiac ECM-based hydrogels improve long term cardiac function post myocardial infarction. *Acta Biomater* **50**, 220-233 (2017). https://doi.org:10.1016/j.actbio.2016.12.015

58. The-Human-Protein-Atlas. *The tissue section - Tissue-based map of the human proteome*, <https://www.proteinatlas.org/ENSG00000164107-HAND2/tissue> (2023).
59. Zhang, X. H. et al. The mesenchymal-epithelial transition during in vitro decidualization. *Reprod Sci* **20**, 354-360 (2013). https://doi.org:10.1177/1933719112472738
60. DeMayo, F. J. & Lydon, J. P. 90 YEARS OF PROGESTERONE: New insights into progesterone receptor signaling in the endometrium required for embryo implantation. *J Mol Endocrinol* **65**, T1-T14 (2020). https://doi.org:10.1530/JME-19-0212
61. Yu, J. J. et al. IL15 promotes growth and invasion of endometrial stromal cells and inhibits killing activity of NK cells in endometriosis. *Reproduction* **152**, 151-160 (2016). https://doi.org:10.1530/REP-16-0089
62. Bellelis, P. et al. Interleukin-15 and Interleukin-7 are the Major Cytokines to Maintain Endometriosis. *Gynecol Obstet Invest* **84**, 435-444 (2019). https://doi.org:10.1159/000496607
63. Liu, H. et al. HAND2 loss-of-function mutation causes familial dilated cardiomyopathy. *Eur J Med Genet* **62**, 103540 (2019). https://doi.org:10.1016/j.ejmg.2018.09.007
64. Giroud, M. et al. HAND2 is a novel obesity-linked adipogenic transcription factor regulated by glucocorticoid signalling. *Diabetologia* **64**, 1850-1865 (2021). https://doi.org:10.1007/s00125-021-05470-y
65. Yuan, Z. et al. Epigenetic silencing and tumor suppressor gene of HAND2 by targeting ERK signaling in colorectal cancer. *Cell Communication and Signaling* **20** (2022). https://doi.org:10.1186/s12964-022-00878-4
66. Zeng, G. G., Li, H. & Tang, C. K. HAND2-AS1: A novel therapeutic target for atherosclerosis. *Int J Cardiol* **360**, 76 (2022). https://doi.org:10.1016/j.ijcard.2022.05.045
67. Ma, L., He, S., Li, H., Zhang, S. & Yin, Y. HAND2-AS1 targeting miR-1208/SIRT1 axis alleviates foam cell formation in atherosclerosis. *Int J Cardiol* **346**, 53-61 (2022). https://doi.org:10.1016/j.ijcard.2021.11.019
68. Su, Y. et al. Mesenchymal stem cell-originated exosomal lncRNA HAND2-AS1 impairs rheumatoid arthritis fibroblast-like synoviocyte activation through miR-143-3p/TNFAIP3/NF-kappaB pathway. *J Orthop Surg Res* **16**, 116 (2021). https://doi.org:10.1186/s13018-021-02248-1
69. Liu, S. & Li, Y. LncRNA HAND2-AS1 attenuates glioma cell proliferation, invasion and migration by targeting CDK6. *Neurol Res* **44**, 677-683 (2022). https://doi.org:10.1080/01616412.2022.2035620
70. lncRNA HAND2-AS1 Regulates Prostate Cancer Cell Growth Through Targeting the miR-106a-5p/RBM24 Axis [Retraction]. *Onco Targets Ther* **15**, 133-134 (2022). https://doi.org:10.2147/OTT.S359036
71. Li, L. et al. Long noncoding RNA HAND2AS1/miR106a/PTEN axis resensitizes cisplatinresistant ovarian cells to cisplatin treatment. *Mol Med Rep* **24** (2021). https://doi.org:10.3892/mmr.2021.12402
72. Gokulnath, P. et al. Long Non-Coding RNA HAND2-AS1 Acts as a Tumor Suppressor in High-Grade Serous Ovarian Carcinoma. *Int J Mol Sci* **21** (2020). https://doi.org:10.3390/ijms21114059
73. Chen, M. J., Song, Z. W., Fei, J. G. & Chen, F. Long non-coding RNA HAND2-AS1: A potential therapeutic target in the treatment of gastric cancer? *Dig Liver Dis* **54**, 148 (2022). https://doi.org:10.1016/j.dld.2021.10.007
74. Shan, L., Liu, W. & Zhan, Y. LncRNA HAND2-AS1 exerts anti-oncogenic effects on bladder cancer via restoration of RARB as a sponge of microRNA-146. *Cancer Cell Int* **21**, 361 (2021). https://doi.org:10.1186/s12935-021-02063-y
75. Gao, Y., Zou, T., Liang, W., Zhang, Z. & Qie, M. Long non-coding RNA HAND2-AS1 delays cervical cancer progression via its regulation on the microRNA-21-5p/TIMP3/VEGFA axis. *Cancer Gene Ther* **28**, 619-633 (2021). https://doi.org:10.1038/s41417-020-00243-y
76. Gong, J., Fan, H., Deng, J. & Zhang, Q. LncRNA HAND2-AS1 represses cervical cancer progression by interaction with transcription factor E2F4 at the promoter of C16orf74. *J Cell Mol Med* **24**, 6015-6027 (2020). https://doi.org:10.1111/jcmm.15117
77. Xing, L. et al. LncRNA HAND2-AS1 suppressed the growth of triple negative breast cancer via reducing secretion of MSCs derived exosomal miR-106a-5p. *Aging (Albany NY)* **13**, 424-436 (2020). https://doi.org:10.18632/aging.202148
78. Ding, J. et al. Identification of key lncRNAs in the tumorigenesis of intraductal pancreatic mucinous neoplasm by coexpression network analysis. *Cancer Medicine* **9**, 3840-3851 (2020). https://doi.org:10.1002/cam4.2927
79. Wang, Y. et al. LncRNA HAND2-AS1 promotes liver cancer stem cell self-renewal via BMP signaling. *EMBO J* **38**, e101110 (2019). https://doi.org:10.15252/embj.2018101110
80. Jing, G. Y., Zheng, X. Z. & Ji, X. X. lncRNA HAND2-AS1 overexpression inhibits cancer cell proliferation in hepatocellular carcinoma by downregulating RUNX2 expression. *Journal of Clinical Laboratory Analysis* **35** (2021). https://doi.org:10.1002/jcla.23717
81. Yan, D., Jin, F. & Lin, Y. lncRNA HAND2-AS1 Inhibits Liver Cancer Cell Proliferation and Migration by Upregulating SOCS5 to Inactivate the JAK-STAT Pathway. *Cancer Biother Radiopharm* **35**, 143-152 (2020). https://doi.org:10.1089/cbr.2019.2958
82. Al-Azab, M. et al. Indian Hedgehog regulates senescence in bone marrow-derived mesenchymal stem cell through modulation of ROS/mTOR/4EBP1, p70S6K1/2 pathway. *Aging (Albany NY)* **12**, 5693-5715 (2020). https://doi.org:10.18632/aging.102958

 doi:10.20944/preprints202309.1783.v1